

# Scalings for fragments produced from drop breakup in shear flow with inertia

Yuriko Y. Renardy

*Department of Mathematics and ICAM, 460 McBryde Hall, Virginia Tech, Blacksburg, Virginia 24061-0123*

Vittorio Cristini

*Department of Chemical Engineering and Materials Science, 151 Amundson Hall, 421 Washington Avenue S.E., University of Minnesota, Minneapolis, Minnesota 55455-0132*

(Received 27 June 2000; accepted 30 April 2001)

When a drop is sheared in a matrix liquid, the largest daughter drops are produced by elongative end pinching. The daughter drop size is found to scale with the critical drop size that would occur under the same flow conditions and fluid properties. Daughter drop volumes saturate to just below 60% of the critical volume as the mother drop size increases. For large Reynolds number, the daughter drop radius scales with the  $-\frac{1}{3}$  case power of the capillary number when the Reynolds number is fixed.

© 2001 American Institute of Physics. [DOI: 10.1063/1.1384469]

## I. INTRODUCTION

We envision a laboratory experiment in which a spherical drop is suspended in a matrix liquid of the same viscosity and density and sheared.<sup>1-6</sup> The velocity field, in the absence of the drop, is  $\mathbf{u} = \dot{\gamma}z\mathbf{i}$ , where  $\dot{\gamma}$  is the imposed shear rate. The fluid properties and flow strength are chosen fixed, while the drop size is varied. For Stokes flow, drop deformation is characterized by the capillary number  $Ca = \mu \dot{\gamma}a / \sigma$ , where  $\mu$  is the viscosity,  $a$  is the initial radius of the drop, and  $\sigma$  is interfacial tension. We denote by  $Ca_c$  the critical capillary number, above which the drop breaks up; the corresponding critical radius is denoted  $a_c$ . The maximum stable drop size is attained at  $Ca_c$ . Above the critical capillary number, the drop elongates, bulbs form at the ends, and these produce the largest daughter drops. It is known that the daughters then stabilize in the flow, and hence their radii  $D$  must be, at most, the critical radius. Their capillary number  $Ca_D = (D/a)Ca$ , where  $D$  is the daughter drop radius, satisfies

$$Ca_D \leq Ca_c. \quad (1.1)$$

Just above the critical capillary number, the daughter drops are roughly 50% of the original volume  $(4/3)\pi a^3$ . If the mother drop radius is increased to drive the capillary number farther above  $Ca_c$ , then it is shown in Ref. 5 for Stokes flow that the volume of the daughter drops becomes insensitive to the mother drop size. It saturates at a value roughly equal to 73% of the critical volume  $(4/3)\pi a_c^3$ , corresponding to  $Ca_D \approx 0.9Ca_c$ . How do these features change at nonzero Reynolds numbers, for which the breakup is due to inertia, as well as to the competition between interfacial tension and shear stress? In this paper, we address the answer to this question.

A full numerical simulation of the initial value problem, for nonzero Reynolds number, is conducted with a VOF-CSF scheme.<sup>7-10</sup> The performance of our code SURFER++ is documented in Refs. 11-13. The plate separation is  $L_z$ , and

the computational box  $L_x \times L_y \times L_z$  has periodic boundary conditions in the horizontal directions.

In addition to the capillary number, we also have the Reynolds number  $Re = \rho \dot{\gamma} a^2 / \mu$ . We define  $Re_D = Re(D^2/a^2)$  for the daughter drop of radius  $D$ . In the laboratory experiment that we envision, just the initial drop size is varied. The parameters are then related by  $Re/Ca^2 = K$ , where  $K = \rho \sigma^2 / (\mu^3 \dot{\gamma})$  is a constant. Figure 1 illustrates this parabola (dashed) in the  $Re$  vs  $Ca$  plane, together with the critical curve (solid) determined in Ref. 6. The intersection of these curves occurs at  $Ca_c$ . The circles on the parabola represent values for the mother drop. Figure 2 shows snapshots of the first daughter drops pinching off from those mother drops. For barely supercritical capillary numbers, the drop breaks after only a modest elongation; two daughter drops of about half the mother's volume and a short neck result from the breakup event. At larger capillary numbers, the drop becomes highly elongated, and the neck has a larger volume. In this case, the neck undergoes subsequent breakups, leading to the formation of several satellites.

## II. DAUGHTER DROP SIZE

For the experiment in Fig. 2, the daughter drop capillary number approaches 0.129 (asterisks in Fig. 1). The critical capillary number from Fig. 1 lies between 0.154 and 0.155. Thus, the daughter volume quickly saturates to 59% of the critical volume for larger capillary numbers, with  $Ca_D = 0.84Ca_c$ .

Figure 3 gives critical conditions and data on daughter drops. At the points represented by + and  $\circ$ , a full simulation of the initial value problem was conducted with our code SURFER++. At the  $(Re, Ca)$  values given by +, the simulation resulted in breakup, and the Reynolds number and capillary number for the daughter drops,  $(Re_D, Ca_D)$ , are plotted as asterisks. At the points given by  $\circ$ , the drop did not break up. Additional datasets for daughter drops, computed with mother drops farther above critical conditions, are also

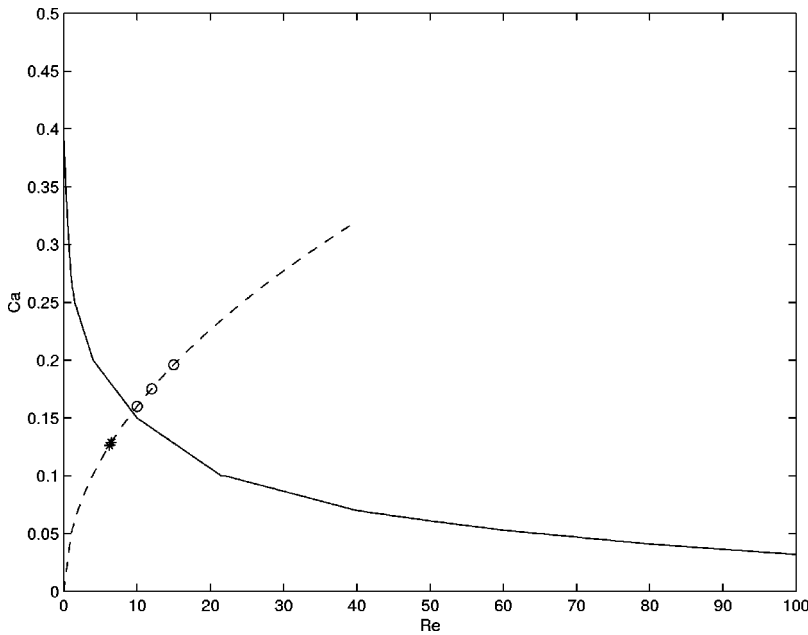


FIG. 1. Here  $Re$  vs  $Ca$  for the critical curve (solid);  $Re=K \cdot Ca^2$  (dashed),  $K=391$ , follows an experiment with fluid properties and flow strength fixed, while the radius of the mother drop varies. Circles represent the mother drop data for Fig. 2. Asterisks denote daughter drop data  $Re_D$  vs  $Ca_D$ .

included in this figure. The line at large Reynolds number represents the inviscid limit.<sup>6</sup> The dashed line represents the parabola  $Re=K \cdot Ca^2$  from Fig. 1.

The offset between the critical curve and that for the daughter drop data is  $\log Ca_c - \log Ca_D$  measured along this parabola, which in Fig. 3 becomes a line parallel to the dashed line. By marking this difference, and projecting it onto the y axis, we find the offset to vary between 0.08 and 0.1, yielding daughter drop volumes of between roughly

50% and 60% of the critical volume. These daughter drops are therefore smaller than those reported for Stokes flow in Ref. 5.

### III. LARGE REYNOLDS NUMBER SCALING

Figure 4 illustrates higher Reynolds numbers, and the manner in which daughter drop data scale with the critical drop volume. The mother drop data are given by  $\circ$  in (a) and daughter drop data by asterisks; these cluster to a single point as the capillary number of the mother drop increases. In (b), we display the ratio of volumes for the daughter drop to critical versus mother drop to critical. The daughter volumes quickly saturate to approximately 57% of the critical volume.

For large Reynolds numbers, the Reynolds stress is of order  $\rho|\mathbf{v}|^2 \sim \rho \dot{\gamma}^2 a^2$ . This is balanced by capillary stresses of order  $\sigma/a$ . The critical condition is, upon division by the viscous stress  $\mu \dot{\gamma}$ ,  $Re \sim 1/Ca$ .<sup>6</sup> In fact, the ratio of inertial to capillary forces is the Weber number  $We = Re Ca$ . The inviscid limit law is approximately  $We = Re Ca = 3.3$ . When the daughter drops are in this asymptotic range, we have  $Re_D \cdot Ca_D = Re \cdot Ca \cdot (D^3/a^3)$ , which yields  $Ca \cdot D^3 = \text{const}$  when the flow Reynolds number and the initial radius are fixed. Figure 5 demonstrates this scaling for the daughter drop radii at  $Re=50$ . The scaling is also verified for Fig. 4, which represents variation of  $Re$  and  $Ca$  along the parabola of fixed physical parameters.

Our computational results are given for plate separation  $L_z=8a$ , spatial periodicity  $L_y=4a$ ,  $L_x$  chosen appropriately large, the mesh  $\Delta x = \Delta y = \Delta z = a/8$ ,  $\dot{\gamma} = 1$ ,  $a = 0.125$ , and time steps  $10^{-3} \dot{\gamma}^{-1}$ , unless otherwise indicated. Convergence tests for the daughter drop size were conducted by varying the mesh, the time step, and the computational domain. These are documented in Table I.

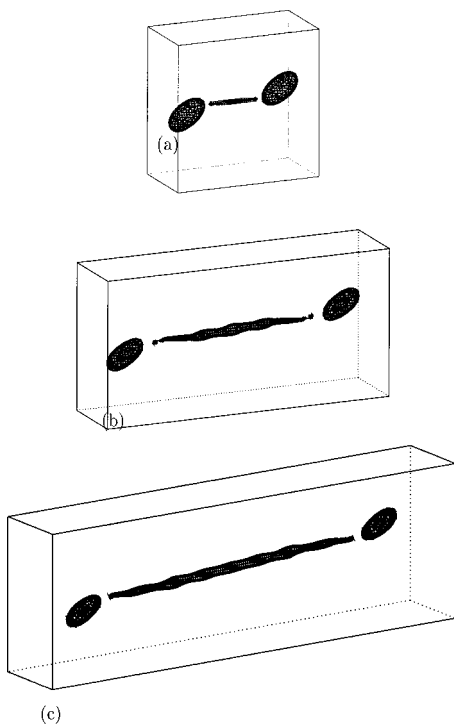


FIG. 2. Pinch-off of daughter drops is shown for the mother drop data ( $\circ$ ) in Fig. 1. (a)  $Re=10$ ,  $Ca=0.16$ ,  $t=19.5$  s. (b)  $Re=12$ ,  $Ca=0.1753$ ,  $t=18$  s. (c)  $Re=15$ ,  $Ca=0.196$ ,  $t=18.6$  s.

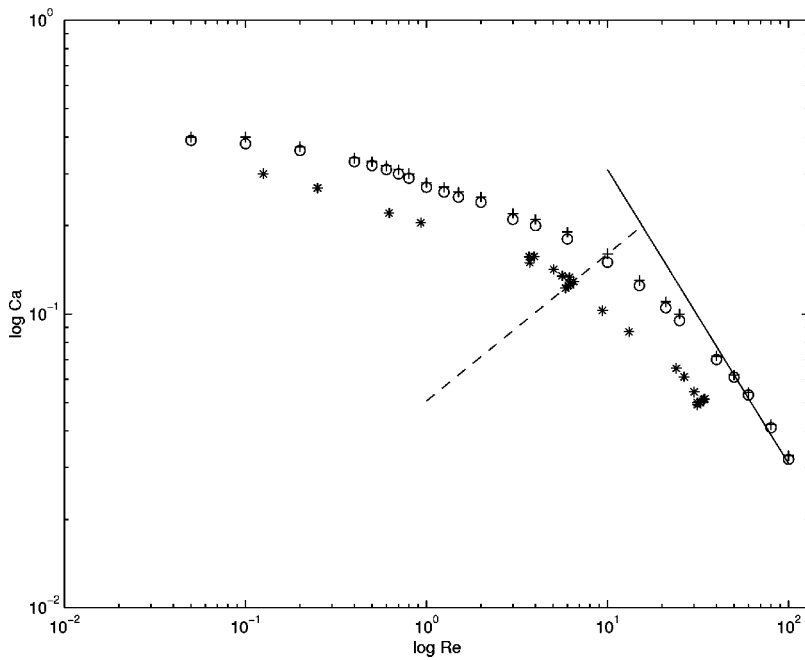


FIG. 3. A log-log plot of  $Re$  vs  $Ca$ ,  $\lambda = 1$ , equal densities. +, drop breakup,  $\circ$ , steady-state solution. Asterisks denote the daughter drop  $Re_D$  vs  $Ca_D$  for mother drops above critical. The solid line represents  $Re \cdot Ca = \text{const}$ , and the dashed line is  $Re/Ca^2 = \text{const}$ .

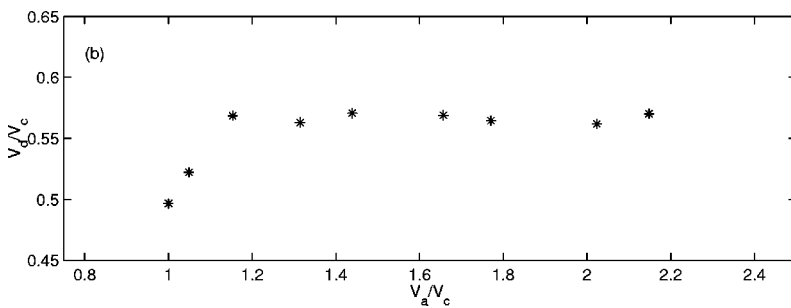
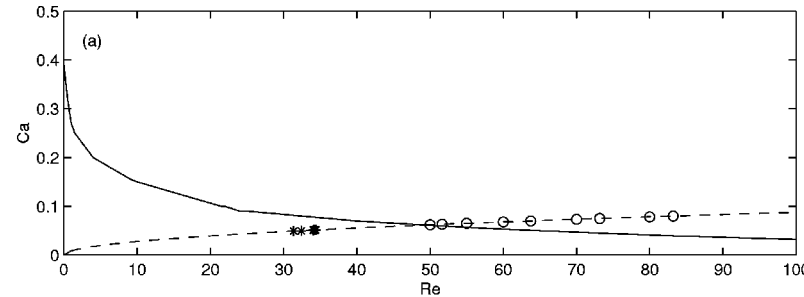


FIG. 4. (a) The solid line represents the critical curve in the  $Re$ - $Ca$  plane. The dashed line represents  $Re = K \cdot Ca^2$ ,  $K = 13\,007$ , for an experiment with fluid properties and flow strength fixed, while the radius of the mother drop varies. Circles represent mother drop data. Asterisks denote daughter drop data ( $Re_D$ ,  $Ca_D$ ); these cluster to a saturated value (34, 0.051). (b) The ratio of volumes of (mother drop)/(critical drop),  $V_a/V_c$ , vs (daughter drop)/(critical drop),  $V_D/V_c$ , with critical conditions at  $Ca \approx 0.062$ . Daughter drop volumes quickly saturate to roughly 57% of the critical volume.

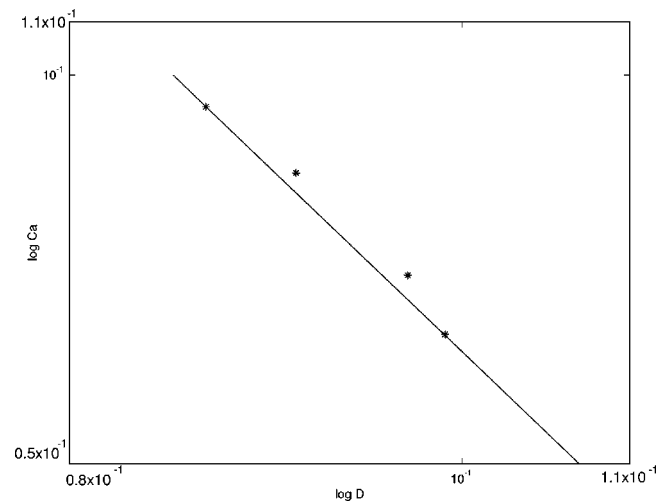


FIG. 5. Flow capillary number  $Ca$  daughter drop radius  $D$  at  $Re = 50$ . The line is  $Ca \cdot D^3 = \text{const}$ .

#### IV. CONCLUSIONS

Our focus in this study is the production of the first daughter drops, under simple shear for finite Reynolds number. The liquids have equal viscosity and density. The relevant microphysical parameters are the Reynolds number and capillary number. Direct numerical simulation is used to determine that the size of the daughter drops saturates, as the capillary number is increased, to under 60% of the critical size; this is smaller than the 73% reported for Stokes flow. Our simulations have been tested for convergence with respect to spatial and temporal refinements, and with respect to changes in the size of the computational box. In order to avoid interactions with neighbors in the periodic array of drops, the computational box must be chosen sufficiently large. The level of accuracy in the predicted volumes reported in this paper is within 1% for lower  $Re$  and  $Ca$  and

TABLE I. Results of numerical simulations for (daughter drop radius)/(mother drop radius) vs mesh and computational box. The first row for each case is cell size  $\Delta x = \Delta y = \Delta z = a/8, a = 0.125$ . (a)  $Re = 10, Ca = 0.16$ . The refinements in space and time show that the spatial mesh and time step used in row 1 produce converged results. Convergence with respect to the computational box size for row 1 is established to 1%. (b)  $Re = 10, Ca = 0.25$ . (c)  $Re = 83.25, Ca = 0.08$ . The most refined case used 36 h with 32 processors on Origin 2000.

	Box	Mesh	Time step	D/a
a	$1 \times 0.5 \times 1$	$64 \times 32 \times 64$	$10^{-3}$	0.788
	$1 \times 0.5 \times 1$	$96 \times 32 \times 64$	$10^{-3}$	0.788
	$1 \times 0.5 \times 1$	$96 \times 64 \times 96$	$10^{-3}$	0.789
	$1 \times 0.5 \times 1$	$64 \times 32 \times 64$	$0.5 \times 10^{-3}$	0.788
	$1.5 \times 0.5 \times 1$	$96 \times 32 \times 64$	$10^{-3}$	0.782
	$2.0 \times 0.5 \times 1$	$128 \times 32 \times 64$	$10^{-3}$	0.780
	$1 \times 1 \times 1$	$64 \times 64 \times 64$	$10^{-3}$	0.790
	$1 \times 1.5 \times 1$	$64 \times 96 \times 64$	$10^{-3}$	0.790
	$1 \times 0.5 \times 1.5$	$64 \times 32 \times 96$	$10^{-3}$	0.788
	$1 \times 0.5 \times 2$	$64 \times 32 \times 128$	$10^{-3}$	0.788
b	$3 \times 0.5 \times 1$	$192 \times 32 \times 64$	$10^{-3}$	0.628
	$3 \times 1 \times 1$	$256 \times 64 \times 64$	$10^{-3}$	0.626
	$4 \times 0.5 \times 1$	$256 \times 32 \times 64$	$10^{-3}$	0.629
c	$3 \times 0.5 \times 1$	$192 \times 32 \times 64$	$10^{-3}$	0.643
	$3 \times 0.5 \times 1$	$256 \times 32 \times 64$	$10^{-3}$	0.632
	$4 \times 1 \times 1$	$256 \times 64 \times 64$	$0.5 \times 10^{-3}$	0.646

8% for the higher end. It is expected that when higher Reynolds numbers or capillary numbers are addressed, that more refinements will be needed. The exploration of satellite distributions will be the subject of future investigation.

## ACKNOWLEDGMENTS

This research was sponsored by National Science Foundation Grants No. NSF-CTS 9612308, No. NSF-INT 9815106, No. NSF-CTS 0090381, No. NSF-DMS SCREMS, and the Illinois NCSA under Grants No. CTS990010N, No.

CTS990059N, and No. CTS990063N, and utilized the NCSA SGI Origin 2000. We are grateful to the Interdisciplinary Center for Applied Mathematics for the use of their Origin 2000. We thank Michael Renardy for discussions, Stephane Zaleski for the use of SURFER, and Jie Li for help with SURFER++. Acknowledgment is made to the donors of The Petroleum Research Fund, administered by the ACS, for partial support of this research.

<sup>1</sup>H. P. Grace, "Dispersion phenomena in high viscosity immiscible fluid systems and application of static mixers as dispersion devices in such systems," *Chem. Eng. Commun.* **14**, 225 (1982).

<sup>2</sup>C. R. Marks, "Drop breakup and deformation in sudden onset strong flows," Ph.D. thesis, University of Maryland at College Park, 1998.

<sup>3</sup>V. Cristini, J. Blawdziewicz, and M. Loewenberg, "Drop breakup in three-dimensional viscous flows," *Phys. Fluids* **10**, 1781 (1998).

<sup>4</sup>S. Guido and M. Villone, "Three-dimensional shape of a drop under simple shear flow," *J. Rheol.* **42**, 395 (1998).

<sup>5</sup>V. Cristini, "Drop dynamics in viscous flow," Ph.D. thesis, Yale University, 2000.

<sup>6</sup>Y. Renardy and V. Cristini, "Effect of inertia on drop breakup under shear," *Phys. Fluids* **13**, 7 (2001).

<sup>7</sup>B. Lafaurie, C. Nardone, R. Scardovelli, S. Zaleski, and G. Zanetti, "Modelling merging and fragmentation in multiphase flows with SURFER," *J. Comput. Phys.* **113**, 134 (1994).

<sup>8</sup>J. Li, "Calcul d'interface affine par morceaux (piecewise linear interface calculation)," *C. R. Acad. Sci. Paris* **320**, 391 (1995).

<sup>9</sup>J. Li, "Résolution numérique de l'équation de Navier-Stokes avec reconnexion d'interfaces. Méthode de suivi de volume et application à l'atomisation," Ph.D. thesis, Université Pierre et Marie Curie, 1996.

<sup>10</sup>R. Scardovelli and S. Zaleski, "Direct numerical simulation of free surface and interfacial flow," *Annu. Rev. Fluid Mech.* **31**, 567 (1999).

<sup>11</sup>J. Li, Y. Renardy, and M. Renardy, "Numerical simulation of breakup of a viscous drop in simple shear flow through a volume-of-fluid method," *Phys. Fluids* **12**, 269 (2000).

<sup>12</sup>J. Li and Y. Renardy, "Numerical study of flows of two immiscible liquids at low Reynolds number," *SIAM Rev.* **42**, 417 (2000).

<sup>13</sup>Y. Renardy and J. Li, "Parallelized simulations of two-fluid dispersions," *SIAM News*, in Applications on Advanced Architecture Computers, edited by G. Astfalk, 1 December, 2000.